Catena 163 (2018) 111–122

Contents lists available at ScienceDirect

Catena

journal homepage: www.elsevier.com/locate/catena

Estimating soil total nitrogen in smallholder farm settings using remote sensing spectral indices and regression kriging

Yiming Xu[a,b,c,*], Scot E. Smith[b,c], Sabine Grunwald[b,d], Amr Abd-Elrahman[c,e], Suhas P. Wani[f], Vimala D. Nair[b,g]

[a] Department of Environmental Science and Engineering, Beijing Technology and Business University, Beijing 100048, China
[b] School of Natural Resource and Environment, University of Florida, 103 Black Hall, PO Box 116455, Gainesville, FL 32611, USA
[c] School of Forest Resources and Conservation – Geomatics Program, University of Florida, 301 Reed Lab, PO Box 110565, Gainesville, FL 32611-0565, USA
[d] Pedometrics, Landscape Analysis and GIS Laboratory, Soil and Water Sciences Department, University of Florida, 2181 McCarty Hall, PO Box 110290, Gainesville, FL 32611, USA
[e] Gulf Coast REC/School of Forest Resources and Conservation – Geomatics Program, University of Florida, 1200 N. Park Road, Plant City, FL 33563, USA
[f] International Crops Research Institute for the Semi-Arid Tropics (ICRISAT), Patancheru, 502324 Hyderabad, India
[g] Soil and Water Sciences Department, 2181 McCarty Hall, PO Box 110290, University of Florida, Gainesville, FL 32611, USA

ARTICLE INFO

Keywords:
Digital Soil Mapping
Remote sensing
Smallholder farm
South India
Soil total nitrogen
Spatial resolution

ABSTRACT

Mapping soil nutrients can help smallholder farmers identify soil nutrient status and implement site-specific soil management schemes. In the past, Digital Soil Mapping has seldom been utilized to guide soil nutrient management in smallholder farm settings in South India. The objective of this research was to analyze the spatial resolution effects of different remote sensing images on soil total nitrogen (TN) prediction models in two smallholder villages, Kothapally and Masuti in South India. Regression kriging (RK) was used to characterize the spatial pattern of TN in the topsoil (0–15 cm) by incorporating spectral indices with different spatial resolutions. The results suggested that soil moisture, vegetation, and soil crusts can contribute to the conservation of soil TN in both study areas. Soil prediction models with different spatial resolutions showed a similar spatial pattern of soil TN. The results also demonstrated that the effect of very fine spatial remote sensing spectral data inputs does not always lead to an increase of soil prediction model performance. A RapidEye-based (5 m) soil TN prediction model had lower prediction accuracy than a Landsat 8-based (30 m) soil TN prediction model in Masuti. WorldView-2/GeoEye-1/Pleiades-1A-based (2 m) soil TN prediction models had the highest prediction accuracy in both study areas. The spectral indices based on new bands of WorldView-2 such as coastal, yellow, red edge, and new near infrared bands had relatively strong correlations with soil TN. The utilization of Very High Spatial resolution images such as WorldView-2 in Digital Soil Mapping could improve soil model performance and spatial characterization. Remote sensing-based soil prediction models have high potential to be widely applied in smallholder farm settings.

1. Introduction

Low and erratic precipitation, drought stress, high temperatures, low biomass, and low soil productivity have major impacts on crop yields in arid and semi-arid farmland in South India (Srinivasarao et al., 2013). Soil nutrient storage is essential and important in semi-arid tropical soils, especially those that are used to maintain food security and soil security in smallholder farm settings. Unlike research focusing on soil sampling and traditional soil laboratory analysis (Ouyang et al., 2013; Venkanna et al., 2014), Digital Soil Mapping (DSM) utilizes categorical and continuous environmental variables to predict soil properties on multiple scales (McBratney et al., 2003; Xu et al., 2017) and is more practical, economical, and suitable for sustainable soil management. However, the application of Digital Soil Mapping (DSM) in smallholder farm settings worldwide is only in its beginning stages due to lack of financial and technical support and historical datasets.

Remote sensing images can provide soil-landscape information such as soil moisture (Bertoldi et al., 2014), vegetation indices (Kross et al., 2015), and land surface temperature (Weng et al., 2014), and are widely utilized in DSM research (Gray et al., 2016; Nigel and Rughooputh, 2010). The past few decades have seen the emergence of various new remote sensing products, which can provide soil-landscape

* Corresponding author at: Department of Environmental Science and Engineering, Beijing Technology and Business University, Beijing 100048, China.
E-mail addresses: xuyiming@btbu.edu.cn (Y. Xu), sesmith@ufl.edu (S.E. Smith), sabgru@ufl.edu (S. Grunwald), aamr@ufl.edu (A. Abd-Elrahman), s.wani@cgiar.org (S.P. Wani), vdn@ufl.edu (V.D. Nair).

https://doi.org/10.1016/j.catena.2017.12.011
Received 11 May 2017; Received in revised form 4 December 2017; Accepted 10 December 2017

information at various scales. Remote sensing images such as Landsat 8 images (30 m) are easily obtained throughout the world. Commercial remote sensing satellites such as WorldView-2 (2 m) and SPOT 5 (10 m) also provide detailed landscape information at relatively fine spatial resolution. As a result, there is a trade-off between choosing fine spatial resolution and coarse spatial resolution remote sensing imagery in DSM.

Some research has indicated advantages to the use of fine spatial resolution images for soil prediction in terms of error assessment and accuracy (Sumfleth and Duttmann, 2008; Vaudour et al., 2013). Other research demonstrated that the highest spatial resolution environmental variables may not always produce the most accurate soil prediction. According to Schmid et al. (2008), ASTER images (30 m) have longer spectral domain and more bands than IKONOS images (4 m). They also have higher prediction capability than IKONOS images in predicting soil classes. Kim and Zheng (2011) demonstrated that fine scale topographic information is not always optimal for understanding soil spatial variability. However, there has been little research analyzing the effects of remote sensing spectral indices with fine to medium spatial resolution (2 m to 30 m) on soil prediction models in regions such as smallholder farm settings.

Unlike ordinary kriging, regression kriging includes deterministic and stochastic components (Hengl et al., 2007). The deterministic component is often a multi-linear regression model between the target soil property and auxiliary environmental variables such as vegetation indices and land use types (Samuel-Rosa et al., 2015). The stochastic component is a spatially correlated random field of residuals from the deterministic component. This spatially correlated random component is usually fitted by variogram and interpolated by ordinary regression (Mora-Vallejo et al., 2008). Regression kriging has been widely applied in the DSM domain (Kuriakose et al., 2009; Mishra et al., 2012; Sun et al., 2012), and has attained better prediction results compared with ordinary kriging (Hengl et al., 2007; Mirzaee et al., 2016). The objectives of this research were to: 1) characterize the spatial pattern of soil Total Nitrogen (TN) in two smallholder villages, Kothapally and Masuti, South India and 2) test and evaluate the spatial resolution effects of spectral indices from Landsat 8 (30 m), RapidEye (5 m), and WorldView-2/GeoEye-1/Pleiades-1A (2 m) on soil TN prediction models in both study areas.

2. Material and methods

2.1. Description of the study areas

Kothapally is a smallholder village located in Ranga Reddy District, Telangana State, India (Fig. 1). It experiences a hot and dry semi-arid climate with an annual rainfall of 802 mm (Sreedevi et al., 2004). Cotton (*Gossypium hirsutum*) and rice (*Oryza sativa*) are the major crops planted in the rainy season. Sorghum (*Sorghum bicolar*) is the predominant crop type in the dry season. The monsoon season is from June to September with the precipitation averaging 755 mm. Vertisols are the major soil type in Kothapally. A detailed description of Kothapally is given by Xu et al. (2017).

Masuti is another smallholder village located in Basavana Bagevadi Tehsil, Bijapur District, Karnataka State, located in South India (Fig. 1). It is 513 km from the state capital, Bangalore. It also experiences a semi-arid climate with temperature variations between 20 °C and 42 °C. The annual rainfall ranges from 569 to 595 mm. The soils in this area vary between dark greyish brown and dark brown to dark reddish brown. Soil texture varies from loam to clay according to investigation by the International Crops Research Institute for the Semi-Arid Tropics (ICRISAT). Sorghum (*Sorghum bicolar*), tomato (*Lycopersicon esculentum* var. *esculentum*), and onion (*Allium cepa*) are the three major crops in the dry season (Table 1). Cotton (*Gossypium hirsutum*), rice (*Oryza sativa*), and maize (*Zea mays*) are the three major crops in the rainy season (Table 1).

2.2. Soil sampling and laboratory analysis

Soil samples were divided into four classes (green, dark, light, and intermediate areas) based on unsupervised classification application in the ERDAS 2011 software (Earth Resource Data Analysis System Inc., Atlanta, GA). Based on the four classes of soil, a stratified random sampling method was performed in ArcMap 10 (Environmental Systems Resource Institute, ArcMap 10.0 ESRI, Redlands, California) using the "SamplingTool_10" (Buja and Menza, 2013) add-in. In total, 255 soil samples at 0–15 cm were collected in Kothapally in May 2012, and 259 soil samples at 0–15 cm were collected in Masuti from February to March 2013 by the ICRISAT and the University of Florida (Fig. 1). Geographic attributes of each soil sample point such as x and y coordinates, were obtained from a Differential Global Positioning System (DGPS) with sub-meter accuracy (Trimble Navigation Ltd., Sunnyvale, California, USA). GPS post-correction was performed by Aimil Ltd. (www.aimil.com) in Hyderabad, India. Site-specific descriptions, including soil types, crop types, soil color and tillage methods, were recorded at each sampling point. After air-drying for one week, all the soil samples in both study areas were sieved through a 2-mm sieve, then analyzed for soil TN based on a concentration basis (mg kg^{-1}) (Krom, 1980) in ICRISAT.

2.3. Remote sensing data collection and processing

Cloud-free satellite remote sensing imagery, including one WorldView-2 image (2 m), one GeoEye-1 image (2 m), two RapidEye images (5 m), and two Landsat 8 images (30 m) in Kothapally, and one WorldView-2 image, one Pleiades-1A image (2 m), two RapidEye images, and two Landsat 8 images in Masuti, were acquired to extract environmental variables in soil TN prediction models (Table 2). Advanced Spaceborne Thermal Emission and Reflection Radiometer (ASTER) Global Digital Elevation Model (DEM) data were obtained in order to extract topographic attributes in both study areas. Table 2 lists all the satellite remote sensing images in the two study areas.

The original pixel values of raw remote sensing images are Digital Numbers (DNs). Radiometric calibration was applied to transform the DNs to top-of-atmosphere spectral radiance using different algorithms depending on the remote sensing products. Atmospheric correction was utilized to convert all the spectral radiance images into surface reflectance images using the Fast Line-of-Site Atmospheric Analysis of Spectral Hypercubes (FLAASH) tool in the ENVI 5.0 software (Exelis Visual Information Solutions, Boulder, Colorado).

2.4. Spectral indices extraction

Multiple spectral indices were extracted from Landsat 8, RapidEye, WorldView-2, GeoEye-1 and Pleiades-1A in the two study areas. Topographic attributes such as elevation (m), slope (degree), aspect (degree), flow direction, and flow accumulation were extracted from the ASTER Global DEM. Table 3 lists all the environmental variables including spectral indices, topographic attributes and geographic attributes in this research. Selected environmental variables were incorporated into the soil TN prediction models.

2.5. Regression kriging

The ordinary kriging method predicts the soil property by calculating the weighted average of the observations (Webster and Oliver, 2001):

$$\hat{z}(s_0) = \sum_{i=1}^{n} \lambda_i * z(s_i) \quad (1)$$

where $\hat{z}(s_0)$ is the predicted value of the target soil properties at an unvisited location s_0, given its coordinates, the sample $z(s_0)$, $z(s_0)$, …, z

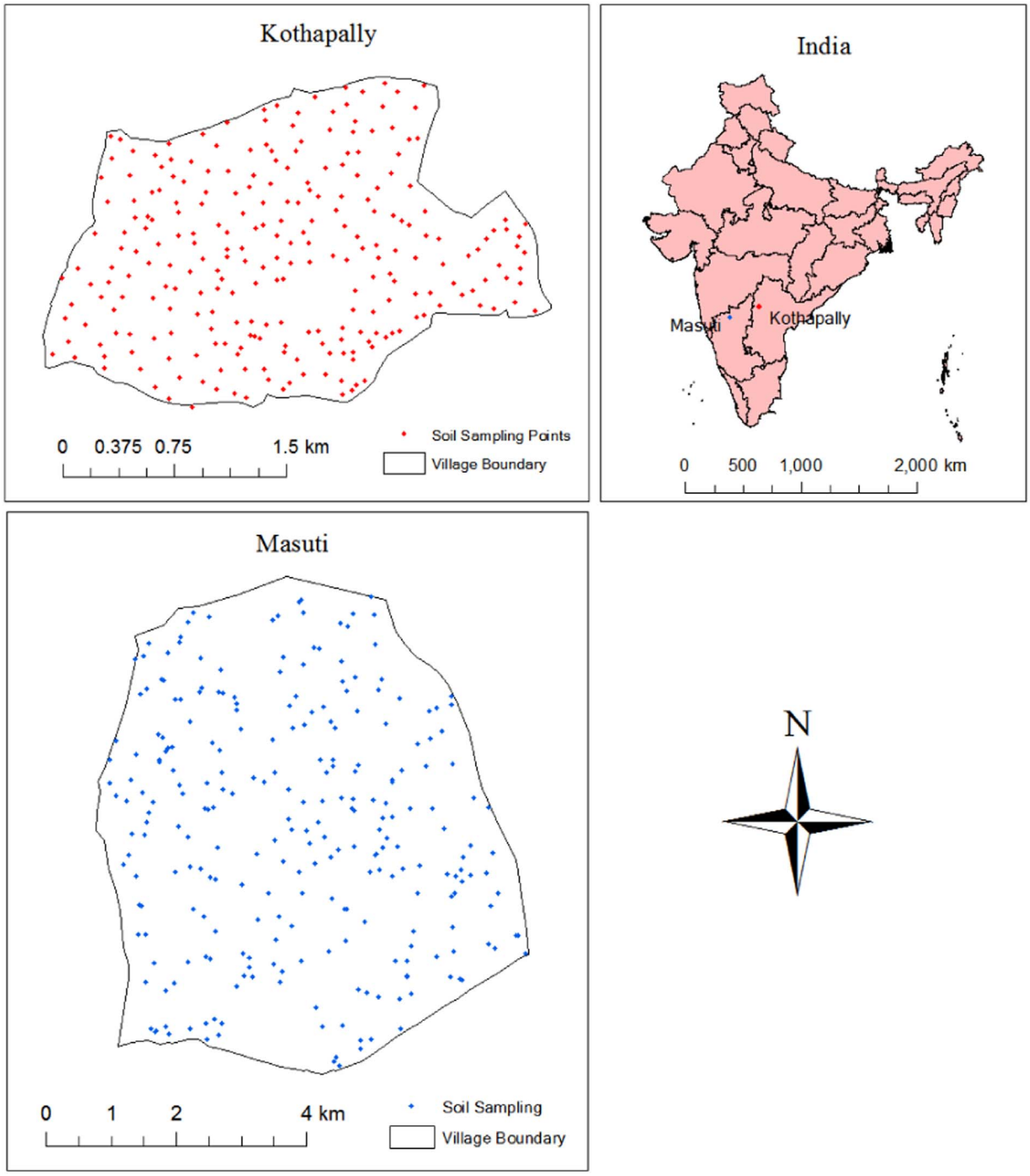

Fig. 1. The boundary and soil samplings of Kothapally and Masuti Village.

Table 1
Description of soil samples.

	Kothapally	Masuti
Soil types	Vertisols	Vertisols, Entisols
Crop types	Major types: Cotton, rice, sorghum Other types: Beet, bitter gourd, eggplant, carrot, chiles, chickpea, cucumber, coriander, flowers, limes, maize, mango, okra, onion, potato, pigeon pea, turmeric, safflower, tomato	Major types: Cotton, rice, maize, sorghum, tomato, onion Other types: Banana, chickpea, eggplant, groundnut, millet, onion, pigeon pea, peanut, sugarcane, safflower, sunflower, wheat
Land use	Grassland land, fallow land, farmland	Forest Land, fallow land, grassland, bare land, farmland
Soil color	dark greyish brown, dark brown, dark reddish brown	dark greyish brown, dark brown, dark reddish brown
Tillage methods	Rainfed, Irrigation	Rainfed, Irrigation

Table 2
Environmental variables from remote sensing images.

Remote sensing images (acquisition date)	Abbreviation	Spatial resolution (m)
Kothapally		
Landsat 8 image (2013-4-13)	LTa	30
Landsat 8 image (2013-4-29)	LTb	30
RapidEye image (2010-4-19)	REa	5
RapidEye image (2013-2-24)	REb	5
WorldView-2 image (2011-12-14)	WVa	2
GeoEye-1 image (2011-1-21)	GE	2
Masuti		
Landsat 8 image (2013-4-20)	LTc	30
Landsat 8 image (2013-5-22)	LTd	30
RapidEye image (2012-12-11)	REc	5
RapidEye image (2013-4-13)	REd	5
WorldView-2 image (2011-2-28)	WVb	2
Pleiades-1A image (2013-3-3)	PL	2

Bands of Landsat 8: Coastal, Blue, Green, Red, Near Infrared (NIR), Short Wavelength Infrared band 1, Short Wavelength Infrared band 2, Panchromatic, Cirrus, Long Wavelength Infrared band 1, Long Wavelength Infrared band 2.
Bands of RapidEye: Blue, Green, Red, Red edge, NIR.
Bands of WorldView-2: Coastal, Blue, Green, Yellow, Red, Red edge, NIR band1, NIR band2.
Bands of GeoEye-1 and Pleiades-1A: Blue, Green, Red, NIR.

(s_0), and their coordinates. The weights λ_i are chosen such that the prediction error variance is minimized, yielding weights that depend on the spatial autocorrelation structure of the variable.

The regression approach predicts the soil property by modelling the relationship between the target soil property and auxiliary environmental variables (e.g. spectral indices) at soil sampling locations and, then applying it to unvisited locations using the known value of the auxiliary variables at those locations (Hengl et al., 2007). Multiple linear regression was used to model the relationships between soil TN and spectral indices from different remote sensing images.

Regression kriging (Hengl et al., 2007) combines these two approaches: multiple linear regression is used to fit the explanatory variables, and ordinary kriging is used to fit the residuals of the multiple linear regression:

$$\hat{z}(s_0) = \hat{m}(s_0) + \hat{e}(s_0) = \sum_{k=0}^{p} \beta_k * q_k(s_0) + \sum_{i=1}^{n} \lambda_i * e(s_i) \quad (2)$$

where $\hat{m}(s_0)$ is the fitted drift, $\hat{e}(s_0)$ is the interpolated residual, β_k are the estimated regression coefficients, $q_k(s_0)$ are the values of the environmental variables, and p is the number of predictors or environmental variables. λ_i are the kriging weights determined by the spatial dependence structure of the residual, and $e(s_i)$ is the residual at location s_i. The regression coefficients β_k are estimated from the sample by ordinary least squares (OLS) in this study.

Several R software (R Development Core Team, 2014) packages such as sp., gstat, geoR, rgdal, maptools, and lattice, were utilized to build the regression kriging models and map soil TN.

2.6. Validation of model accuracy

For each soil TN prediction model, all the soil sampling points were randomly split into a calibration set (70%, Kothapally: 179 points, Masuti: 76 points) for model calibration and a validation set (30%, Kothapally: 180 points, Masuti: 79 points) for independent model validation. The Kolmogorov-Smirnov test was applied for the soil calibration and validation sets to ensure that they had the same distribution. A log-transformation was applied to the whole soil dataset, calibration soil data set, and validation soil dataset to ensure the normal distribution of soil data. The coefficient of determination (R^2), root mean squared error (RMSE), and residual prediction deviation (RPD) (Bellon-Maurel et al., 2010) were computed using R software and used

Table 3
Environmental variables from remote sensing images.

Environmental variables	Abbreviation	References
Coastal band reflectance	Coastal	
Blue band reflectance	Blue	
Green band reflectance	Green	
Yelllow band reflectance	Yellow	
Red band reflectance	Red	
Red edge band reflectance	Rededge	
Near Infrared band reflectance	NIR	
Near Infrared band 1 reflectance	NIR1	
Near Infrared band 2 reflectance	NIR2	
Short Wavelength band 1 reflectance	SWIR1	
Short Wavelength band 2 reflectance	SWIR2	
Green/Blue ratio	GB	
Red/Blue ratio	RB	
Red/Green ratio	RG	
Red edge/Blue ratio	REB	
Red edge/Green ratio	REG	
Red edge/Red ratio	RER	
NIR/Blue ratio	NB	
NIR/Green ratio	NG	
NIR/Red ratio	NR	
NIR1/Blue ratio	N1B	
NIR1/Green ratio	N1G	
NIR1/Red ratio	N1R	
NIR1/Red edge ratio	N1RE	
NIR2/Blue ratio	N2B	
NIR2/Green ratio	N2G	
NIR2/Red ratio	N2R	
NIR2/Red edge	N2RE	
NIR2/NIR1 ratio	N2N1	
SW1/Blue ratio	S1B	
SW1/Green ratio	S1G	
SW1/Red ratio	S1R	
SW1/NIR ratio	S1N	
SW2/Blue ratio	S2B	
SW2/Green ratio	S2G	
SW2/Red ratio	S2R	
SW2/NIR ratio	S2N	
SW2/SW1 ratio	S2S1	
Normalized Difference Vegetation Index	NDVI	Rouse et al. (1974)
Normalized Difference Green Index	NDVIg	Gitelson et al. (1996)
Simple Ratio	SR	Cohen (1991)
Transformed Spectral Index	TVI	Nellis and Briggs (1992)
Green Chlorophyll Index	CIg	Gitelson et al. (2005)
Soil Adjusted Vegetation Index	SAVI	Qi et al. (1994)
Atmospherically Resistant Vegetation Index	ARVI	Kaufman and Tanré (1996)
Crust Index	CI	Karnieli (1997)
Modified Chlorophyll Absorption in Reflectance Index	MCARI	Daughtry et al. (2000)
Red-edge Chlorophyll Index	CIr	Gitelson et al. (2005)
Normalized Difference Red-edge Index	NDVIr	Gitelson and Merzlyak (1994), Sims and Gamon (2002)
Transformed Chlorophyll Absorption in Reflectance Index	TCARI	Haboudane et al. (2002)
Moisture Stress Index	MSI	Rock et al. (1986)
Normalized Difference Water Index	NDWI	Gao (1996)
Mid-infrared Index	MidIR	Musick and Pelletier (1988)
Bare Soil Index	BSI	Rikimaru and Miyatake (1997)
Normalized Difference Soil Index	NDSI	Rogers and Kearney (2004)
At-satellite brightness temperature for band 10 (10.30–11.30 μm) (K)	T1	
At-satellite brightness temperature for band 11 (11.50–12.50 μm) (K)	T2	
Elevation (m)	Elevation	
Aspect (degree)	Aspect	
Flow accumulation	FlowAccu	
Flow direction	FlowDir	
Slope (degree)	Slope	

Table 4
Descriptive analysis of original and log-transformed TN.

Location	Transform	Data type	N	Mean	Median	SD	Min	Max	Range	Skew	Kurtosis	CV
Kothapally		Total	255	869	856	221	329	1821	1492	0.47	1.05	0.25
		Calibration	179	874	856	222	400	1821	1421	0.63	1.37	0.25
		Validation	76	856	860	217	329	1507	1178	0.06	− 0.02	0.25
Masuti		Total	259	514	487	186	166	1182	1016	0.59	0.14	0.36
		Calibration	180	514	487	191	166	1182	1016	0.63	0.17	0.37
		Validation	79	515	487	177	206	1059	853	0.47	− 0.12	0.34
Kothapally	$\log_{10}(x)$	Total	255	2.92	2.93	0.11	2.52	3.26	0.74	− 0.46	0.53	0.04
	$\log_{10}(x)$	Calibration	179	2.93	2.93	0.11	2.6	3.26	0.66	− 0.32	0.42	0.04
	$\log_{10}(x)$	Validation	76	2.92	2.93	0.12	2.52	3.18	0.66	− 0.71	0.52	0.04
Masuti	$\log_{10}(x)$	Total	259	2.68	2.69	0.16	2.22	3.07	0.85	− 0.3	− 0.25	0.06
	$\log_{10}(x)$	Calibration	180	2.68	2.69	0.16	2.22	2.98	0.76	− 0.35	− 0.35	0.06
	$\log_{10}(x)$	Validation	79	2.69	2.68	0.17	2.23	3.07	0.84	− 0.21	− 0.15	0.06

Abbreviations: N, number of samples; SD, standard deviation; CV; coefficient of variation.

to compare different regression kriging models.

3. Results

3.1. Descriptive analysis of soil TN

Descriptive analysis of soil TN and log-transformed soil TN is shown in Table 4. TN showed a positive-skewed distribution, with a mean of 869 mg kg^{-1}, a median of 856 mg kg^{-1}, and a range of 1492 mg kg^{-1} in Kothapally. Total nitrogen showed a positive-skewed distribution, with a mean of 514 mg kg^{-1}, a median of 487 mg kg^{-1}, and a range of 1016 mg kg^{-1} in Masuti. The mean of soil TN is lower in Masuti compared to that in Kothapally. After the log-transformation, all the datasets (whole, calibration, and validation) of soil TN were Gaussian distributed in the two study areas.

3.2. Correlation coefficients between soil TN and spectral indices from different remote sensing images

Table 5 shows Spearman's rank correlation coefficients between soil TN and spectral indices from different remote sensing images. The Atmospherically Resistant Vegetation Index (ARVI) and Crust Index (CI) from Landsat 8, RapidEye, WorldView-2, GeoEye-1, and Pleiades-1A showed positive correlations with TN in both study areas. Near-infrared-related spectral indices from all remote sensing images, such as Normalized Difference Vegetation Index (NDVI), Simple Ratio (SR) and Transformed Spectral Index (TVI), and red-edge-related spectral indices from WorldView-2 and RapidEye, such as Normalized Difference Red-edge Index (NDVIr) and Red-edge Chlorophyll Index (CIr), as well as the band ratio between NIR band 2 to red-edge (N2RE), showed relatively strong positive correlations with TN in both study areas. Band ratios such as red to green (RG), red to blue (RB), and short wavelength (SWIR) band 2 to SWIR band 1 (S2S1), as well as the band reflectances such as red band (Red), yellow band (Yellow) and blue band (Blue) from remote sensing images showed relatively strong negative correlations with TN in both study areas. Bare soil indices such as the Bare Soil Index (BSI) and Normalized Difference Soil Index (NDSI) from Landsat 8 showed relatively strong negative correlations with TN in both study areas. Thermal band-related spectral indices from Landsat 8 such as at-satellite brightness temperature for thermal band 1 (10.30–11.30 μm) (T1) and thermal band 2 (11.50–12.50 μm) (T2) also showed relatively strong negative correlations with TN.

3.3. Multiple linear regression models

Six multiple linear regression models between log-transformed TN (calibration soil data set) and spectral indices in Kothapally (K1, K2, K3), and in Masuti (M1, M2, M3) are shown in Table 6. All six multilinear regression models showed relatively low coefficients of determination (< 0.3). Ordinary kriging was performed on the residuals of the six multiple linear regression models. Six regression kriging models of TN based on the multiple linear regression models in Kothapally (KR1, KR2, and KR3) and Masuti (MR1, MR2, and MR3) were built to predict soil TN and characterize the spatial pattern of TN in both study areas (Table 7).

3.4. Characterization of soil TN in smallholder farms

3.4.1. Spatial pattern of TN at different spatial resolutions in Kothapally

Spatial variations of soil TN in Kothapally generally showed a similar pattern in three maps in Fig. 2. Total nitrogen in the southwestern and northern areas of the village was relatively lower compared with other areas. The east-west strip areas in the center of the village and the southeastern area of the village had relatively higher TN. TN variation based on Landsat 8 images (Fig. 2(A)) was smoother than in the other two maps in Fig. 2. The finer characterization of the TN pattern exemplified the advantages of model KR3 (Fig. 2(C)) based on WorldView-2 and GeoEye-1 spectral indices in depicting the TN pattern in small farmlands.

Spatial variation of soil TN in Farmland A (a small farmland in Kothapally) demonstrated the similarities and differences of the three models more clearly (Fig. 3). Generally, Fig. 3(A), (B), and (C) showed relatively low TN in the northwestern and southeastern areas of Farmland A and relatively high TN from the southwest to northeast across Farmland A. Fig. 3(A) generalized the TN distribution, and it may mix the spatial pattern of TN in different field blocks owned by many farmers. Fig. 3(B) had a higher capability to detect the fine variations in Farmland A, such as the fragmented TN pattern across the Farmland A. Fig. 3(C) showed the evident rectangular patchy pattern of TN in each field block, the linear low TN pattern in the western area of Farmland A, and subtle variations of TN in each field block.

3.4.2. Spatial pattern of TN at different spatial resolutions in Masuti

The distribution of TN based on models MR1, MR2 and MR3 showed similar spatial patterns (Fig. 4). Total nitrogen was relatively higher in the southwestern area of the village compared with other areas (Fig. 4). An irrigation channel was located in this region that it may bring more water and increase soil moisture in the region. Total nitrogen was relatively low in the northern area of the village where most of the area was permanently fallow, and the main soil types were Entisols according to the ICRISAT. Venkanna et al. (2014) also concluded that TN was higher in cultivated fields than in permanently fallow soils, and higher under irrigated conditions than under rainfed conditions in the semiarid region of South India. The farmland close to a dam in the north-central area of the village also had relatively high TN. Vertisols are the main soil type in the southern area of the village, and this soil type is rich in montmorillonite clay and has a relatively high exchangeable buffering capacity in South India (Krishna, 2010).

Table 5
Linear correlations between soil TN and spectral indices different remote sensing images.

Kothapally					
Landsat 8		RapidEye		WV and GE	
Index	R	Index	R	Index	R
LTbRG	− 0.419	REbRed	− 0.429	GECI	0.475
LTbARVI	0.409	REbARVI	0.421	GERB	− 0.475
LTaARVI	0.397	REbCI	0.412	GERed	− 0.474
LTbCI	0.390	REbRB	− 0.412	GERG	− 0.440
LTbRB	− 0.390	REbRG	− 0.404	GEBlue	− 0.395
LTaRG	− 0.373	REbBlue	− 0.387	WVaCI	0.393
LTbT2	− 0.373	REbNDVIr	0.385	WVaRB	− 0.393
LTbT1	− 0.368	REbCIr	0.385	GEGreen	− 0.390
LTaCI	0.364	REbNRE	0.385	WVaRG	− 0.372
LTaRB	− 0.364	REaARVI	0.381	GEARVI	0.351
LTbRed	− 0.353	REbNDVI	0.367	WVaRed	− 0.325
LTaRed	− 0.339	REbSR	0.367	WVaYellow	− 0.318
LTbBSI	− 0.318	REbTVI	0.367	GENDVI	0.262
LTaT1	− 0.309	REbNR	0.367	GESR	0.262
LTaMidIR	0.289	REbGreen	− 0.364	GETVI	0.262
Masuti					
Landsat 8		RapidEye		WV and PL	
Index	R	Index	R	Index	R
LTcARVI	0.481	REcCI	0.414	WVbCI	0.45
LTcRG	− 0.481	REcRB	− 0.414	WVbRB	− 0.45
LTcBSI	− 0.478	REcRededge	− 0.388	PLRG	− 0.44
LTdRG	− 0.465	REcRed	− 0.379	PLCI	0.437
LTdCI	0.454	REdRededge	− 0.371	PLRB	− 0.437
LTdRB	− 0.454	REdCI	0.368	PLRed	− 0.424
LTcCI	0.45	REdRB	− 0.368	WVbRG	− 0.417
LTcRB	− 0.45	REcREB	− 0.365	WVbRed	− 0.405
LTdBSI	− 0.447	REcGreen	− 0.351	WVbYellow	− 0.402
LTcRed	− 0.442	REdRed	− 0.346	PLGB	0.397
LTdARVI	0.441	REcGB	− 0.344	PLBlue	− 0.384
LTdRed	− 0.441	REdGreen	− 0.339	WVbN2RE	0.381
LTcSWIR2	− 0.432	REcARVI	0.338	WVbARVI	0.379
LTcNDWI	0.416	REcRG	− 0.335	PLARVI	0.376
LTcMSI	− 0.416	REdGB	− 0.32	PLGreen	− 0.369

Nomenclature of the variables in Table 5: Remote Sensing Image (Abbreviations in Table 2) + Spectral Index (Abbreviations in Table 3). All the spectral indices in Table 5 show significant correlations with soil TN ($p < 0.05$).

Table 6
Multi-linear regression model of soil TN.

Model	Multi-linear regression model	Spatial resolution (m)	R^2
K1	logTN = 6.09 + 1.02*LTbCI-0.014*LTbT2 + 0.07*LTbS2B-0.008*Slope	30	0.22
K2	logTN = 3.16 + 0.21*REaARVI-0.08*REbRed + 0.59*REbCI	5	0.21
K3	logTN = 2.19 + 0.77*GECI-0.01*Slope + 1.45*WVaBlue + 0.37*WVaNDVIr	2	0.26
M1	logTN = 5.90 + 0.44*LTcARVI + 0.15*LTcBSI-0.89*LTcSWIR1-0.01*LTcT1	30	0.24
M2	logTN = 2.77 − 0.23*REcRB + 0.19*REcGB-0.13*REcRededge + 0.15*REcARVI	5	0.20
M3	logTN = 1.13 + 1.02*WVbCI + 0.69*WVbN2RE-0.73*WVbCIr	2	0.31

Venkanna et al. (2014) and Srinivasarao et al. (2009) also indicated that soil organic carbon and soil nitrogen are relatively higher in Vertisols than in other soil types in South India. As a result, the TN in the southern area of the village was relatively higher than in the northern area of the village. Unlike the homogeneous and smooth variation of TN in the 30 m map produced by MR1 (Fig. 4(A)), there is a heterogeneous and fragmented spatial variation of TN in the 2 m map produced by model MR3 (Fig. 4(C)). Fig. 4(A) showed a large continuous area in the northern area of the village containing TN at lower concentrations than 400 mg kg^{-1}. However, Fig. 4(B) and (C) revealed a mosaicked spatial pattern of TN in the northern area of the village.

Table 7
Model validation results of regression kriging models for TN.

Model	Adj R^2	RMSE (mg kg^{-1})	RPD	Spatial resolution (m)
KR1	0.28	179.46	1.16	30
KR2	0.36	167.89	1.24	5
KR3	0.42	159.36	1.31	2
MR1	0.48	146.24	1.33	30
MR2	0.41	148.70	1.30	5
MR3	0.56	130.73	1.49	2

Fig. 5 shows the prediction for TN in Farmland B (a small farmland in Masuti). All three maps in Fig. 5 show relatively low TN in the northern and southeastern Farmland B, and relatively high TN in the western Farmland B. The Landsat 8-based TN map (Fig. 5(A)) only showed a few pixels. The RapidEye-based TN map (Fig. 5(B)) identified high TN in the northern area of Farmland B and a more detailed TN pattern. The WorldView-2/Pleiades-1A-based TN map (Fig. 5(C))

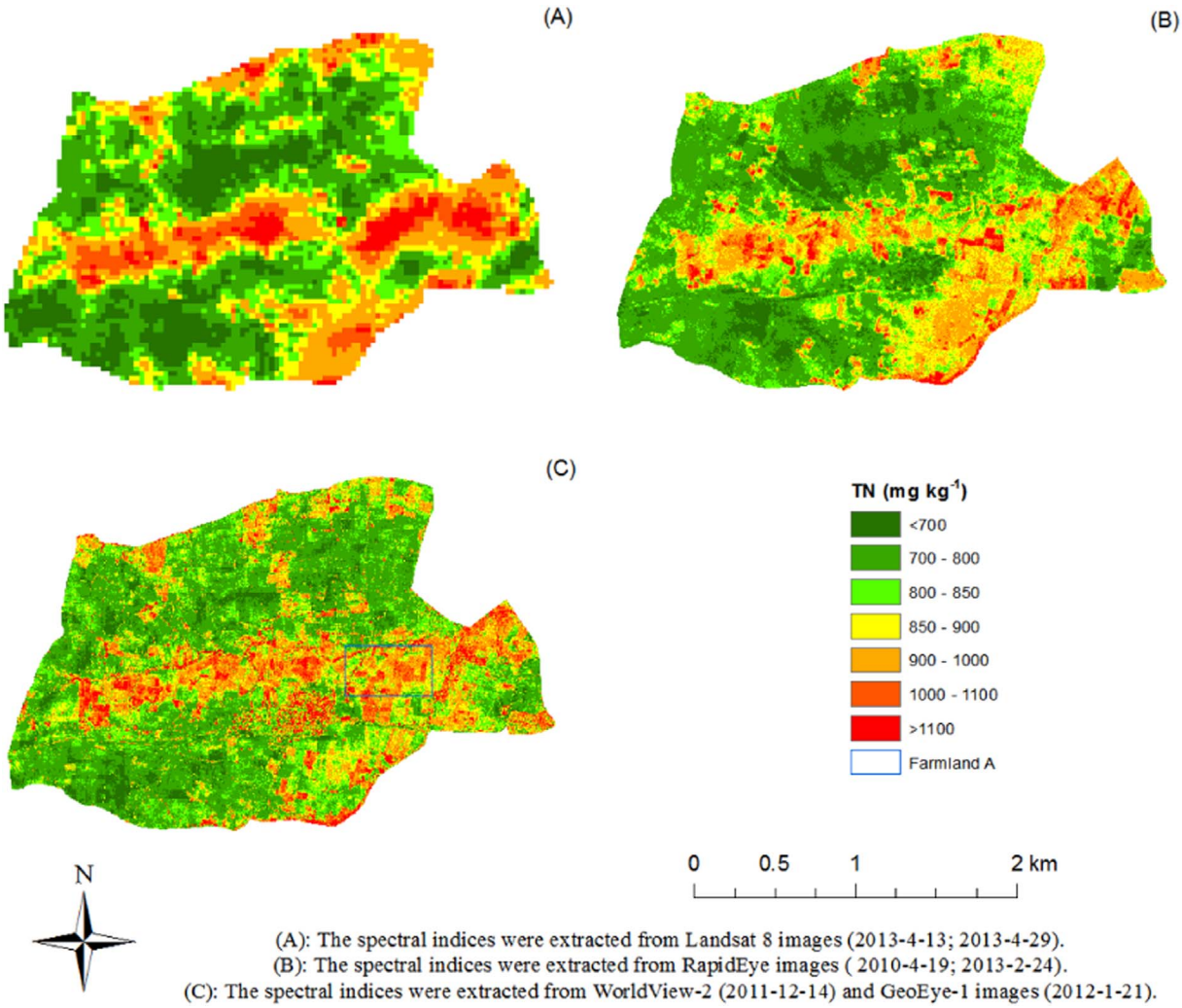

Fig. 2. Soil total nitrogen (TN) prediction at 0–15 cm depth in Kothapally from (A) Model KR1: Regression kriging of TN based Landsat 8 images; (B) Model KR2: Regression kriging model of TN based on RapidEye images; (C) Model KR3: Regression kriging model of TN based on WorldView-2 and GeoEye-1 images.

characterized the gradient variation and fragmented pattern of TN in Farmland B, which demonstrated the paramount advantages of Model MR3 in displaying the TN in different field blocks and depicting the subtle variation of TN in each field block.

3.4.3. Validation of regression kriging model for TN

Table 7 shows the validation results of soil TN prediction models in both study areas. In Kothapally, the RK model of TN based on WorldView-2 and GeoEye-1 images (KR3) attained the highest model fit (R^2 = 0.42) and lowest prediction error (RMSE = 159.36 mg kg^{-1}) compared with the RK models of TN based on Landsat 8 (KR1) and RapidEye (KR2). In Masuti, the Landsat 8-based model MR1 can still attain fair prediction accuracy (R^2 = 0.48; RMSE = 146.24 mg kg^{-1}) regardless of its relatively coarse spatial resolution (30 m). RapidEye-based model MR2 attained lower prediction accuracy (R^2 = 0.41; RMSE = 148.70 mg kg^{-1}) compared with Landsat 8-based model MR1. Model MR3 based on WorldView-2 and Pleiades-1A attained the highest prediction accuracy (R^2 = 0.56; RMSE = 130.73 mg kg^{-1}).

4. Discussion

4.1. Spectral indices with different spatial resolutions

The reflectance of vegetation was low in both blue and red spectrum regions due to the absorption by chlorophyll for photosynthesis. In contrast, the reflectance of bare soil increased steadily in the visible and near-infrared (VNIR) spectral region. Most research has already confirmed that the visible band spectral reflectances of bare soils are higher than those of vegetated areas (Holben, 1986), and the visible band spectral reflectances of relatively dry soils are higher than those of relatively wet soils (Fabre et al., 2015). The strong negative relationship between visible band reflectances and soil TN suggested that less vegetated areas tend to have less soil TN than richly vegetated areas, and drier soils tend to have less soil TN than wetter soils. The Crust Index (CI) and ARVI of different remote sensing images all showed relatively strong positive correlations with TN. As soil crusts contribute to soil stability, soil build-up, soil fertility, and soil water regime in arid and semi-arid areas, the strong positive relationship between CI and TN confirmed the importance of soil crust for soil TN conservation in the study areas. ARVI, which uses the difference in the radiance between the blue and the red channels to correct the radiance in the red channel, is four times less sensitive to atmospheric conditions compared to NDVI (Kaufman and Tanre, 1992). Red-edge measurement is valuable for the assessment of vegetative chlorophyll status and leaf area index independent of ground cover variations (Horler et al., 1983; Mutanga and Skidmore, 2004). The strong correlations between red edge-related indices (e.g., NDVIr and red-edge spectral reflectances) and soil TN in both study areas also suggested that those indices have strong predictive capability in soil TN prediction models in South India.

Spectral indices from SWIR have the potential to provide

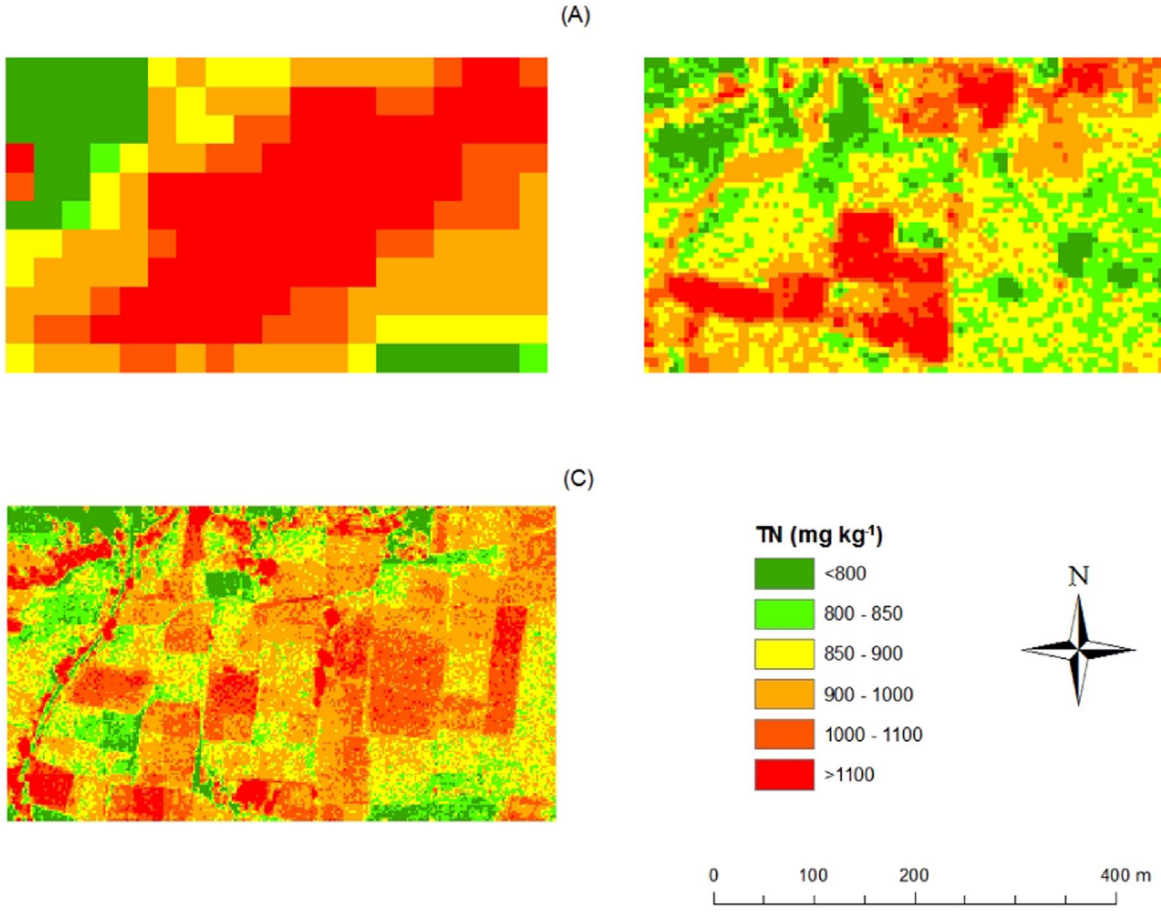

(A): The spectral indices were extracted from Landsat 8 images (2013-4-13; 2013-4-29).
(B): The spectral indices were extracted from RapidEye images (2010-4-19; 2013-2-24).
(C): The spectral indices were extracted from WorldView-2 (2011-12-14) and GeoEye-1 images (2012-1-21).

Fig. 3. Soil TN prediction at 0–15 cm depth in Farmland A from (A) Model KR1; (B) Model KR2; (C) Model KR3 in Kothapally.

information about soil moisture conditions, as water has pronounced absorption features in the SWIR region (van der Meer, 2004). This suggests that the soil water can increase the absorption of SWIR and decrease the reflectance in SWIR region. The strong negative relationship between soil TN and SWIR reflectances suggests the accumulation of soil TN in low SWIR reflectance areas (wet soils or vegetation areas). The results of Musick and Pelletier (1988) showed that the Mid-infrared Index (MidIR, band ratio of SWIR band 1 to SWIR band 2) had a positive relationship with soil water content. The relatively strong positive relationship between the MidIR from Landsat 8 and TN demonstrated the importance of soil water content in retaining soil TN in this area.

The negative correlations between Thermal infrared (TIRS) indices, such as at-satellite brightness temperatures of thermal bands (band 10 and band 11) from Landsat 8 and TN suggested that soils with relatively lower at-satellite brightness temperatures (higher water content) were likely to contain higher TN than soils with relatively higher at-satellite brightness temperatures (lower water content). Many researchers have also tried to estimate soil moisture from at-satellite brightness temperature data using multiple algorithms (Paloscia et al., 2006; Song et al., 2014).

Due to the limited remote sensing images in the two study areas, there is a discrepancy between the acquisition date of the remote sensing images and soil collection time. This problem may explain the low correlations between some spectral indices and soil TN in Table 5 (< 0.4). The spectral behavior of the spectral indices from different remote sensing images is similar. For example, the ARVI and CI from remote sensing images in both study areas all had relatively strong positive correlations with TN. The spectral reflectances and band ratios from remote sensing images in both study areas all had relatively strong negative correlations with TN. These results suggested the transferability of important spectral indices in soil prediction models in different semi-arid smallholder farms. The correlation relationships between multiple spectral indices and soil TN also suggested that soil moisture, vegetation, and soil crusts could contribute to the conservation of soil TN in both study areas. In all, the Crust Index, which showed the soil crust, NIR band-related and red-edge band-related vegetation indices, which reflected the vegetation cover and biomass, and band reflectances and band ratios, which indicated the soil moistures, were the indices that displayed relatively strong correlations with TN and were included in the regression model (Table 6).

4.2. Selection of remote sensing images for Digital Soil Mapping in smallholder farms

Due to the wider spectral range and larger number of spectral bands of the Landsat 8 images, spectral indices from the visible-NIR-SWIR-TIR spectrum region can provide spectral information about soil moisture, vegetation and soil temperature, which affect the spatial pattern of soil properties. In addition, Landsat 8 has higher temporal resolution than commercial satellites and can reflect multi-period soil-landscape information. As a result, models KR1 and MR1 can still attain fair prediction results at a relatively low spatial resolution (30 m). Due to the

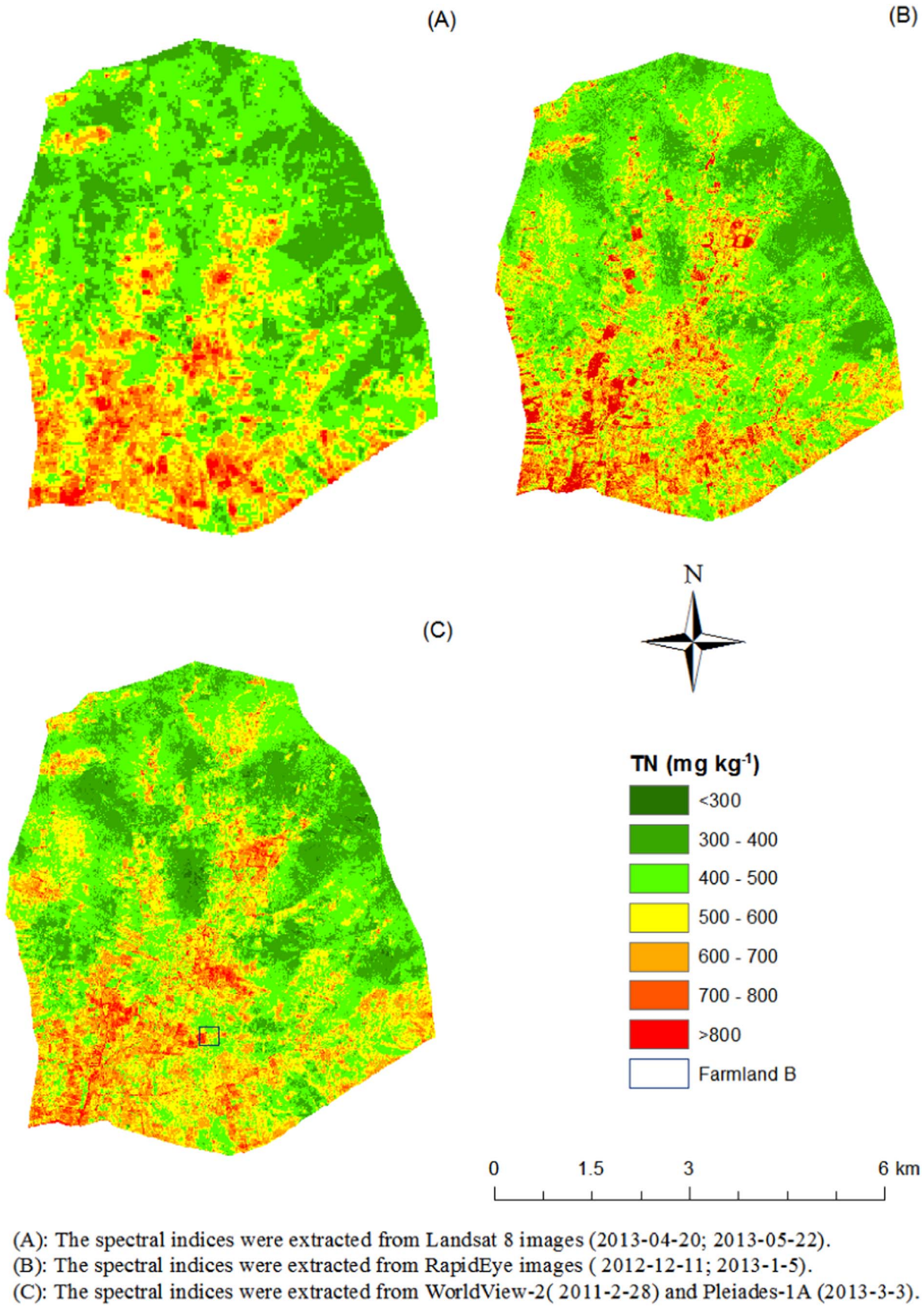

Fig. 4. Soil TN prediction at 0–15 cm depth in Masuti from (A) Model MR1: Regression kriging of TN based Landsat 8 images; (B) Model MR2: Regression kriging model of TN based on RapidEye images; (C) Model MR3: Regression kriging model of TN based on WorldView-2 and Pleiades-1A images.

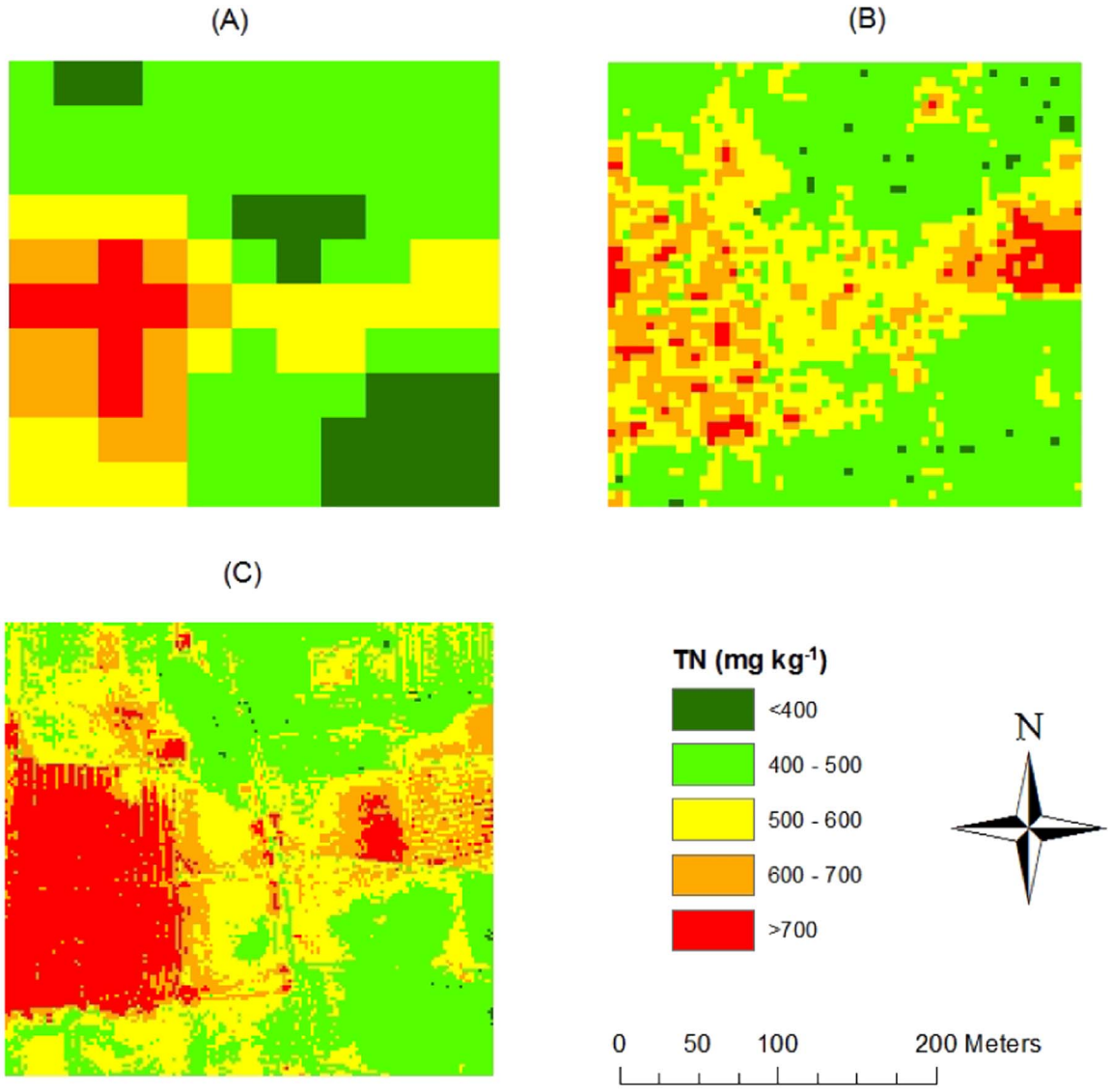

Fig. 5. Soil TN prediction at 0–15 cm depth in Farmland B from (A) Model MR1; (B) Model MR2; (C) Model MR3 in Masuti.

availability of freely available remote sensing images such as Landsat and Sentinels, the application of DSM in data poor regions such as smallholder farms can be promoted with little human and financial support.

The application of Very High Resolution (VHR) remote sensing images in the DSM domain in smallholder farms is in its infancy. The comparison of soil prediction models based on different remote sensing images also suggested that the spectral indices from VHR remote sensing did not necessarily result in higher prediction accuracy for soil prediction models compared with those from medium resolution remote sensing data. For example, the prediction accuracy of Model MR2, based on RapidEye was lower than that of Model MR1, based on Landsat 8. The spatial pattern of soil properties such as TN in smallholder farm settings may also be affected by micro-scale topographic attributes and human agricultural practices. These factors cannot be captured in their entirely by even fine resolution spectral indices.

The complexity and variation of TN in Kothapally (Fig. 2(C)) and Masuti (Fig. 4(C)) confirmed that the soil prediction models based on WorldView-2, GeoEye-1 and Pleiades-1A have paramount advantages over other models in depicting the subtle variation of soil properties in small farmlands. WorldView-2/GeoEye-1/Pleiades-1A-based soil TN prediction models attained the highest model accuracy ($R^2 > 0.4$) in both study areas. WorldView-2 images have a red-edge band (705–745 nm), a new NIR band (860–1040 nm) and finer spatial resolution compared with other images. The WorldView-2 image is the first sensor to include the yellow, red-edge, coastal, two separate NIR and traditional visible bands in a single focal plane (Wolf, 2010). The new coastal band has the potential to produce more spectral indices to reflect subtle moisture differences, such as soil and surface moisture levels, which are not exploitable by traditional Visible-NIR multispectral images (Wolf, 2010). These VHR remote sensing spectral indices can capture more detailed and unmixed spectral and spatial information in fine landscape agricultural fields.

4.3. Site-specific soil management schemes based on DSM in smallholder farms

To help smallholder farmers identify the soil nutrient status in their fields, it is important to map soil nutrients such as soil TN in smallholder villages. Soil TN prediction models only incorporating remote sensing spectral indices can still attain fair prediction accuracy. This research suggests that digital soil models utilizing remote sensing spectral indices from Landsat 8 have a high potential to be widely applied in smallholder farms due to the free acquisition of the images, fine temporal resolution, and fair model performance. Digital soil models utilizing Very High Resolution (VHR) images such as WorldView-2 and Pleiades-1A have a strong capability to characterize the spatial pattern of soil properties in fine scale farmland and provide more site-specific soil recommendations in smallholder farms, due to the fine spatial resolution and fair model performance. As commercial satellites usually required image purchases and more processing time and have limited image acquisitions, the wide application of DSM research based on VHR images in the smallholder farm settings is less practical. Agricultural experts, policymakers and other end-users of DSM can choose different types of Very High Resolution images as options for building soil prediction models, and guide the soil management in smallholder farms according to financial budget and data availability.

In future research, hyperspectral images such as Hyperion, airborne visible/infrared imaging spectrometer (AVIRIS) and Unmanned Aerial Vehicle (UAV)-based remote sensing products also have potential to be utilized in Digital Soil Mapping research and help smallholder farmers implement field-specific soil nutrient management schemes.

5. Conclusions

The results demonstrated that soil moisture, vegetation, and soil crusts could contribute to the conservation of soil TN in both study areas. Soil TN models with different spatial resolutions showed similar spatial patterns of soil TN. The effect of very fine spatial remote sensing spectral data inputs does not always lead to an increase in soil prediction model performance. This research suggested that soil prediction models utilizing satellite imagery-derived spectral indices from Landsat 8 have a high potential to be widely applied in smallholder farm settings due to the free acquisition of images, high temporal resolution and relatively strong prediction capability. Agricultural experts, policymakers and other end-users of DSM can choose different types of Very High Resolution images as options for building soil prediction models, and guide soil nutrient management in smallholder farms according to financial budget and data availability.

Acknowledgements

This work is supported by the grant award no. 1201943 “Development of a Geospatial Soil-Crop Inference Engine for Smallholder Farmers” EAGER National Science Foundation and Research Foundation for Youth Scholars of Beijing Technology and Business University. The soil analysis was performed in the soil laboratory at the International Crops Research Institute for the Semi-Arid Tropics (ICRISAT) in Patancheru/Hyderabad, India. We thank Christopher M. Clingensmith at University of Florida, and other ICRISAT staff members and villagers of Kothapally for support in field sampling. We also thank Yiming Xu's PhD committee member Dr. Thomas K. Frazer for his commitment and guidance. A matching assistantship for Yiming Xu was provided by the School of Natural Resources and Environment, University of Florida, and the China Scholarship Council.

References

Bellon-Maurel, V., Fernandez-Ahumada, E., Palagos, B., Roger, J.-M., McBratney, A., 2010. Critical review of chemometric indicators commonly used for assessing the quality of the prediction of soil attributes by NIR spectroscopy. TrAC Trends Anal. Chem. 29, 1073–1081. http://dx.doi.org/10.1016/j.trac.2010.05.006.

Bertoldi, G., Della Chiesa, S., Notarnicola, C., Pasolli, L., Niedrist, G., Tappeiner, U., 2014. Estimation of soil moisture patterns in mountain grasslands by means of SAR RADARSAT2 images and hydrological modeling. J. Hydrol. 516, 245–257. (Determination of soil moisture: Measurements and theoretical approaches). https://doi.org/10.1016/j.jhydrol.2014.02.018.

Buja, K., Menza, C., 2013. Sampling design tool for ArcGIS: Instruction manual. [for ESRI ArcGIS 10.0 Service Pack 3 or higher]. NOAA/National Centers for Coastal Ocean Science, Silver Spring, MD. 16pp. Accessed September 13, 2016. http://aquaticcommons.org/14676/1/Buja%20and%20Menza%202013.pdf.

Cohen, W.B., 1991. Response of vegetation indices to changes in three measures of leaf water stress. Photogramm. Eng. Remote. Sens. 195–202.

Daughtry, C.S.T., Walthall, C.L., Kim, M.S., de Colstoun, E.B., McMurtrey III, J.E., 2000. Estimating corn leaf chlorophyll concentration from leaf and canopy reflectance. Remote Sens. Environ. 74, 229–239. http://dx.doi.org/10.1016/S0034-4257(00)00113-9.

Fabre, S., Briottet, X., Lesaignoux, A., 2015. Estimation of soil moisture content from the spectral reflectance of bare soils in the 0.4–2.5 µm domain. Sensors 15, 3262–3281. http://dx.doi.org/10.3390/s150203262.

Gao, B., 1996. NDWI—A normalized difference water index for remote sensing of vegetation liquid water from space. Remote Sens. Environ. 58, 257–266. http://dx.doi.org/10.1016/S0034-4257(96)00067-3.

Gitelson, A., Merzlyak, M.N., 1994. Spectral reflectance changes associated with autumn senescence of Aesculus hippocastanum L. and Acer platanoides L. leaves. Spectral features and relation to chlorophyll estimation. J. Plant Physiol. 143, 286–292. http://dx.doi.org/10.1016/S0176-1617(11)81633-0.

Gitelson, A.A., Kaufman, Y.J., Merzlyak, M.N., 1996. Use of a green channel in remote sensing of global vegetation from EOS-MODIS. Remote Sens. Environ. 58, 289–298. http://dx.doi.org/10.1016/S0034-4257(96)00072-7.

Gitelson, A.A., Viña, A., Ciganda, V., Rundquist, D.C., Arkebauer, T.J., 2005. Remote estimation of canopy chlorophyll content in crops. Geophys. Res. Lett. 32, L08403. http://dx.doi.org/10.1029/2005GL022688.

Gray, J.M., Bishop, T.F.A., Wilford, J.R., 2016. Lithology and soil relationships for soil modelling and mapping. Catena 147, 429–440. http://dx.doi.org/10.1016/j.catena.2016.07.045.

Haboudane, D., Miller, J.R., Tremblay, N., Zarco-Tejada, P.J., Dextraze, L., 2002. Integrated narrow-band vegetation indices for prediction of crop chlorophyll content for application to precision agriculture. Remote Sens. Environ. 81, 416–426. http://dx.doi.org/10.1016/S0034-4257(02)00018-4.

Hengl, T., Heuvelink, G.B.M., Rossiter, D.G., 2007. About regression-kriging: from equations to case studies. Comput. Geosci. 33, 1301–1315. (Spatial Analysis Spatial Analysis). https://doi.org/10.1016/j.cageo.2007.05.001.

Holben, B.N., 1986. Characteristics of maximum-value composite images from temporal AVHRR data. Int. J. Remote Sens. 7, 1417–1434. http://dx.doi.org/10.1080/01431168608948945.

Horler, D.N.H., Dockray, M., Barber, J., 1983. The red edge of plant leaf reflectance. Int. J. Remote Sens. 4, 273–288. http://dx.doi.org/10.1080/01431168308948546.

Karnieli, A., 1997. Development and implementation of spectral crust index over dune sands. Int. J. Remote Sens. 18, 1207–1220. http://dx.doi.org/10.1080/014311697218368.

Kaufman, Y.J., Tanre, D., 1992. Atmospherically resistant vegetation index (ARVI) for EOS-MODIS. IEEE Trans. Geosci. Remote Sens. 30, 261–270. http://dx.doi.org/10.1109/36.134076.

Kaufman, Y.J., Tanré, D., 1996. Strategy for direct and indirect methods for correcting the aerosol effect on remote sensing: from AVHRR to EOS-MODIS. Remote Sens. Environ. 55, 65–79. http://dx.doi.org/10.1016/0034-4257(95)00193-X.

Kim, D., Zheng, Y., 2011. Scale-dependent predictability of DEM-based landform attributes for soil spatial variability in a coastal dune system. Geoderma 164, 181–194. http://dx.doi.org/10.1016/j.geoderma.2011.06.002.

Krishna, K.R., 2010. Agroecosystems of South India: Nutrient Dynamics, Ecology and Productivity. Universal-Publishers.

Krom, M.D., 1980. Spectrophotometric determination of ammonia: a study of a modified Berthelot reaction using salicylate and dichloroisocyanurate. Analyst 105, 305–316. http://dx.doi.org/10.1039/AN9800500305.

Kross, A., McNairn, H., Lapen, D., Sunohara, M., Champagne, C., 2015. Assessment of RapidEye vegetation indices for estimation of leaf area index and biomass in corn and soybean crops. Int. J. Appl. Earth Obs. Geoinf. 34, 235–248. http://dx.doi.org/10.1016/j.jag.2014.08.002.

Kuriakose, S.L., Devkota, S., Rossiter, D.G., Jetten, V.G., 2009. Prediction of soil depth using environmental variables in an anthropogenic landscape, a case study in the western Ghats of Kerala, India. Catena 79, 27–38. http://dx.doi.org/10.1016/j.catena.2009.05.005.

McBratney, A.B., Mendonça Santos, M.L., Minasny, B., 2003. On digital soil mapping. Geoderma 117, 3–52. http://dx.doi.org/10.1016/S0016-7061(03)00223-4.

van der Meer, F., 2004. Analysis of spectral absorption features in hyperspectral imagery. Int. J. Appl. Earth Obs. Geoinf. 5, 55–68. http://dx.doi.org/10.1016/j.jag.2003.09.001.

Mirzaee, S., Ghorbani-Dashtaki, S., Mohammadi, J., Asadi, H., Asadzadeh, F., 2016. Spatial variability of soil organic matter using remote sensing data. Catena 145, 118–127. http://dx.doi.org/10.1016/j.catena.2016.05.023.

Mishra, U., Torn, M.S., Masanet, E., Ogle, S.M., 2012. Improving regional soil carbon inventories: combining the IPCC carbon inventory method with regression kriging. Geoderma 189–190, 288–295. http://dx.doi.org/10.1016/j.geoderma.2012.06.022.

Mora-Vallejo, A., Claessens, L., Stoorvogel, J., Heuvelink, G.B.M., 2008. Small scale

digital soil mapping in southeastern Kenya. Catena 76, 44–53. http://dx.doi.org/10.1016/j.catena.2008.09.008.
Musick, H.B., Pelletier, R.E., 1988. Response to soil moisture of spectral indexes derived from bidirectional reflectance in thematic mapper wavebands. Remote Sens. Environ. 25, 167–184. http://dx.doi.org/10.1016/0034-4257(88)90099-5.
Mutanga, O., Skidmore, A.K., 2004. Narrow band vegetation indices overcome the saturation problem in biomass estimation. Int. J. Remote Sens. 25, 3999–4014.
Nellis, M.D., Briggs, J.M., 1992. Transformed vegetation index for measuring spatial variation in drought impacted biomass on Konza Prairie, Kansas. Trans. Kans. Acad. Sci. (1903-) 95, 93–99. http://dx.doi.org/10.2307/3628024.
Nigel, R., Rughooputh, S.D.D.V., 2010. Soil erosion risk mapping with new datasets: an improved identification and prioritisation of high erosion risk areas. Catena 82, 191–205. http://dx.doi.org/10.1016/j.catena.2010.06.005.
Ouyang, W., Xu, Y., Hao, F., Wang, X., Siyang, C., Lin, C., 2013. Effect of long-term agricultural cultivation and land use conversion on soil nutrient contents in the Sanjiang Plain. Catena 104, 243–250. http://dx.doi.org/10.1016/j.catena.2012.12.002.
Paloscia, S., Macelloni, G., Santi, E., 2006. Soil moisture estimates from AMSR-E brightness temperatures by using a dual-frequency algorithm. IEEE Trans. Geosci. Remote Sens. 44, 3135–3144. http://dx.doi.org/10.1109/TGRS.2006.881714.
Qi, J., Chehbouni, A., Huete, A.R., Kerr, Y.H., Sorooshian, S., 1994. A modified soil adjusted vegetation index. Remote Sens. Environ. 48, 119–126. http://dx.doi.org/10.1016/0034-4257(94)90134-1.
R. Development Core Team, 2014. R: A Language and Environment for Statistical Computing. R Foundation for Statistical Computing, Vienna, Austria.
Rikimaru, A., Miyatake, S., 1997. Development of forest canopy density mapping and monitoring model using indices of vegetation, bare soil and shadow. Available at. http:\www.gisdevelopment.net/aars/acrs/1997/ts5/index.shtmm.
Rock, B.N., Vogelmann, J.E., Williams, D.L., Vogelmann, A.F., Hoshizaki, T., 1986. Remote detection of forest damage. Bioscience 36, 439–445. http://dx.doi.org/10.2307/1310339.
Rogers, A.S., Kearney, M.S., 2004. Reducing signature variability in unmixing coastal marsh thematic mapper scenes using spectral indices. Int. J. Remote Sens. 25, 2317–2335. http://dx.doi.org/10.1080/01431160310001618103.
Rouse, J.W., Haas, R.H., Schell, J.A., Deering, D.W., 1974. Monitoring vegetation systems in the great plains with Erts. In: NASA Special Publication. 351. pp. 309.
Samuel-Rosa, A., Heuvelink, G.B.M., Vasques, G.M., Anjos, L.H.C., 2015. Do more detailed environmental covariates deliver more accurate soil maps? Geoderma 243–244, 214–227. http://dx.doi.org/10.1016/j.geoderma.2014.12.017.
Schmid, T., Koch, M., DiBlasi, M., Hagos, M., 2008. Spatial and spectral analysis of soil surface properties for an archaeological area in Aksum, Ethiopia, applying high and medium resolution data. Catena 75, 93–101. http://dx.doi.org/10.1016/j.catena.2008.04.008.
Sims, D.A., Gamon, J.A., 2002. Relationships between leaf pigment content and spectral reflectance across a wide range of species, leaf structures and developmental stages. Remote Sens. Environ. 81, 337–354. http://dx.doi.org/10.1016/S0034-4257(02)00010-X.
Song, C., Jia, L., Menenti, M., 2014. Retrieving high-resolution surface soil moisture by downscaling AMSR-E brightness temperature using MODIS LST and NDVI data. IEEE J. Sel. Top. Appl. Earth Obs. Remote Sens. 7, 935–942. http://dx.doi.org/10.1109/JSTARS.2013.2272053.
Sreedevi, T., Shiferaw, B., Wani, S., 2004. Adarsha Watershed in Kothapally Understanding the Drivers of Higher Impact: Global Theme on Agroecosystems Report no. 10.
Srinivasarao, C., Vittal, K.P.R., Venkateswarlu, B., Wani, S.P., Sahrawat, K.L., Marimuthu, S., Kundu, S., 2009. Carbon stocks in different soil types under diverse rainfed production systems in tropical India. Commun. Soil Sci. Plant Anal. 40, 2338–2356. http://dx.doi.org/10.1080/00103620903111277.
Srinivasarao, C., Venkateswarlu, B., Lal, R., Singh, A.K., Kundu, S., 2013. Chapter five - sustainable management of soils of dryland ecosystems of india for enhancing agronomic productivity and sequestering carbon. In: Sparks, D.L. (Ed.), Advances in Agronomy. Academic Press, pp. 253–329.
Sumfleth, K., Duttmann, R., 2008. Prediction of soil property distribution in paddy soil landscapes using terrain data and satellite information as indicators. Ecol. Indic. 8, 485–501. http://dx.doi.org/10.1016/j.ecolind.2007.05.005.
Sun, W., Minasny, B., McBratney, A., 2012. Analysis and prediction of soil properties using local regression-kriging. Geoderma 171–172, 16–23. http://dx.doi.org/10.1016/j.geoderma.2011.02.010.
Vaudour, E., Bel, L., Gilliot, J.M., Coquet, Y., Hadjar, D., Cambier, P., Michelin, J., Houot, S., 2013. Potential of SPOT multispectral satellite images for mapping topsoil organic carbon content over Peri-urban croplands. Soil Sci. Soc. Am. J. 77, 2122. http://dx.doi.org/10.2136/sssaj2013.02.0062.
Venkanna, K., Mandal, U.K., Raju, A., Sharma, K., Adake, R.V., Pushpanjali, B., Reddy, B.S., Masane, R.N., Venkatravamma, K., Babu, B., 2014. Carbon stocks in major soil types and land-use systems in semiarid tropical region of southern India. Curr. Sci. 106, 604–611.
Webster, R., Oliver, M.A., 2001. Geostatistics for Environmental Scientists (Statistics in Practice).
Weng, Q., Fu, P., Gao, F., 2014. Generating daily land surface temperature at Landsat resolution by fusing Landsat and MODIS data. Remote Sens. Environ. 145, 55–67. http://dx.doi.org/10.1016/j.rse.2014.02.003.
Wolf, A., 2010. Using Worldview 2 Vis-Nir MSI Imagery to Support Land Mapping and Feature Extraction Using Normalized Difference Index Ratios. In: Proceedings of SPIE. 8390. Accessed September 13, 2016. http://www.exelisvis.com/portals/0/pdfs/envi/8_bands_Antonio_Wolf.pdf.
Xu, Y., Smith, S.E., Grunwald, S., Abd-Elrahman, A., Wani, S.P., 2017. Incorporation of satellite remote sensing pan-sharpened imagery into digital soil prediction and mapping models to characterize soil property variability in small agricultural fields. ISPRS J. Photogramm. Remote Sens. 123, 1–19. http://dx.doi.org/10.1016/j.isprsjprs.2016.11.001.